A Novel Three-Phase Oak Ridge AC / DC Converter for Wireless EV Charger Applications

Erdem Asa, Omer C. Onar, Veda P. Galigekere, Gui-Jia Su, and Burak Ozpineci
Buildings and Transportation Science Division, Oak Ridge National Laboratory
National Transportation Research Center, Knoxville, TN 37932, USA
E-mail: asae@ornl.com

Abstract— **In this paper, a novel three-phase converter is proposed for ac to dc wireless power transfer (WPT) systems for electric vehicle (EV) charging applications. The proposed innovative solution, called as Oak Ridge Converter, reduces the design complexity and cost by eliminating the front-end converter stage compared to the conventional systems. Additionally, grid side requirements can be met with the proposed creative concept. In this concept, the three-phase single-stage Oak Ridge Converter directly converts the 60 Hz grid frequency into high-frequency voltage and utilizes hybrid grid-source and high-frequency to realize power transfer from AC source through resonant network and coupling coils to the battery load. Simulation validation of the proposed three-phase system is currently being carried on and the results will be will be provided to validate the theoretical studies with the input of 277 $V_{AC,RMS}$ and output of 675 V_{DC} at 35 kW power. The system current total harmonic distortion (THD) is measured 5% with a power factor (PF) of 0.98 and overall hardware development of the system that will be used for experiments is presented.**

Keywords— Oak Ridge, resonant, converter, grid, high frequency, wireless, EV, charger

I. INTRODUCTION

Wireless power transfer (WPT) technology for electric vehicle (EV) charging applications is very convenient for industrial and commercial systems considering any environment and weather conditions [1]-[2]. As EV charger power density increases, WPT technology is more suitable in higher power applications that wired/plug-in systems would be more difficult to deploy due to the wire thickness and weight. For instance, for a 350 kW charger, the input current from the 480V 3-phase input would be close to 500A per phase that requires bulky cables and plugs; thus plug-in chargers would be prohibitive at these high power levels. Moreover, high power charging system may require a special infrastructure with a dedicated plug and receptacle that users might not be allowed to handle high power equipment [3]-[4]. Therefore, WPT technology offers highly reliable, flexible, convenient, and a safe method for EV charging applications thorough inductively coupled coils within an air gap for stationary and dynamic charging systems [5].

WPT systems are usually consists of minimum two converter stages on the primary-side including a grid connected rectifier stage and a high-frequency inverter [6]-[7]. Considering the size, weight, volume, and cost of the WPT system from grid to the battery, a direct ac to ac system (60 Hz grid frequency to 85 kHz high-frequency switching) on the primary-side would be more cost effective without requiring the ac / dc conversion stage. This approach would also reduce the dc link bulk capacitor requirement. Matrix converter topologies have been studied to transfer the energy from directly ac grid without front-end rectifiers with power factor correction (PFC) in several WPT applications [8]-[11]. Although the dc link requirement can be eliminated with matrix converter structure, the converter configuration is complicated to analyze the circuit switching transitions; especially due to the fact that usually three-phase bi-directional semiconductor switches are employed to achieve the single-phase WET system. Moreover, these converters require complex commutation strategy to control the switches during the transition. Due to their high input current harmonic distortions as reported in [12]-[13], matrix converters are not suitable for charging systems; especially for long operating periods; however, they might be used for energy injection to the load for a short period of time such as in dynamic wireless charging applications. Bi-directional matrix converter topologies have also been investigated between grid and vehicle battery for WPT applications in [14]-[15]. Single-phase integrated converter topologies are explored with Z-source circuit and bridgeless PFC converter for WPT application in [16]

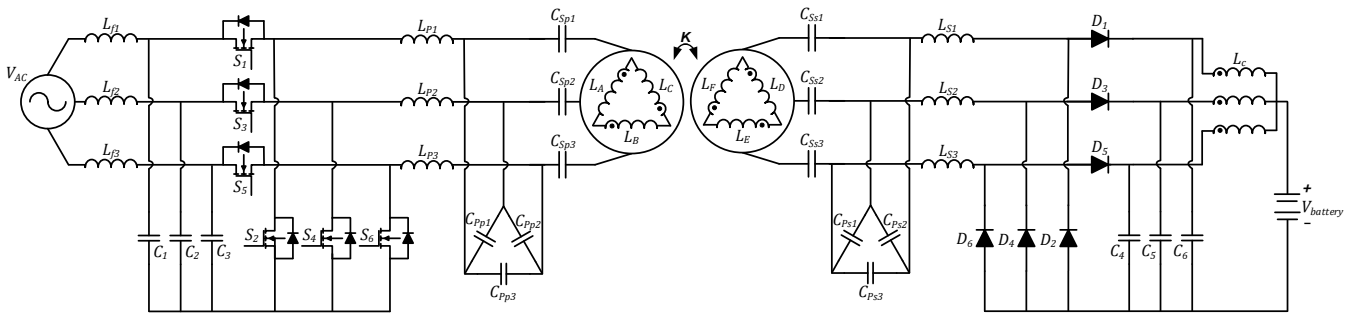

Fig. 1. The proposed three-phase Oak Ridge converter for wireless EV charging applications .

Although the converter construction provides less active and passive components than the conventional two-stage converters, their grid-side THD values are above the standard limitations. Authors in [17] proposed single stage WPT system through three -phase grid and six-pulse rectifier by using T-type topology. The converter can maintain the low THD and high PF; however, the converter efficiency is low.

This study presents a novel three phase Oak Ridge ac / dc wireless power transfer topology for EV charging applications. In the proposed converter topology, 60 Hz ac grid frequency can be converted to the high frequency ac with a single power conversion stage for wireless power transfer through three-phase coupler coils and then it is converted to the dc on the secondary-side. Compared to the conventional wireless EV charger systems, the innovative solution reduces the design complexity and cost and also meets the grid-side PF and THD requirements at the constant operating frequency. Three-phase converter switches are driven with 50 % duty cycle and 120^{o} phase shifted PWM complementary gate signals during positive and negative half line cycles of three-phase grid for upper and lower switching legs. The system state model and theoretical analysis of the converter are provided for delta connected three phase LCC - LCC tuning topology. The simulation result of the presented converter will validate the system performance at power of 35 kW from an input of three phase source 277 $V_{AC,RMS}$ with the output voltage of 675 V_{DC}. The system overall design parameters are presented for simulation analysis and simulation results show PF of 0.98 and the input current THD of 5% at full load.

II. The Proposed System and System Analysis

The proposed three phase Oak Ridge ac / dc converter topology is demonstrated for the WET applications in Fig. 1. As seen from the figure, the invented technology allows transferring power directly from grid to the EV battery without a front-end PFC converter. The system contains a three-phase filter inductor, three-phase active switches, three-phase LCC / LCC resonant compensation circuit, a pair of three-phase coupling coils, a six-pulse (three-phase) rectifier, output decoupling filter capacitor, and a three-phase common mode choke filter, and battery load. The grid-side frequency and high frequency switching are superimposed through the three-phase LCC resonant compensation circuits and coupling coils and rectified through the output rectifier and decoupling capacitors and common mode choke to the EV battery load.

The proposed converter switch transition and state analysis are presented the behavior of the three-phase system in Fig. 2 and Fig. 3, respectively. To simplify the circuit analysis, input and output filter losses are assumed to be negligible, three phase active switches and gate drive system are ideal and switching losses are not concerned. Also, the secondary side rectifier diode losses are assumed negligible. The oak ridge converter system is analyzed in the following operation modes.

Mode 1 [t_0<t<t_1]

The current flow of the active switches, decoupling capacitors, resonant compensation, and coupler coil are presented during first interval in Fig. 2.a. While the phase - B grid voltage is in positive half-cycle and phase - A and phase - C are in negative half-cycle, the active switches S_2, S_4, and S_5 are turned on-state and body diode of switch S_2 is on-state as shown in Fig. 3. The coupling capacitors C_2 is charged and C_1, C_3 are discharged to the input filter L_{f1}, L_{f3} and active switch S_5. The current flows through the first and third phase series inductors L_{P1}, L_{P3} and returns from the second phase series inductor L_{P2}. The parallel capacitor between first and second phases C_{Pp1} is charged and C_{Pp2} and C_{Pp3} are discharged through the second phase series inductor L_{P2} and series capacitor C_{Sp2}. In this way, the series capacitor C_{Sp2} is charged through the coupler transformer. The current flows from phase - B winding L_B and phase - C windings L_C and returns to phase - A windings L_A in coupler transformer and series capacitors C_{Sp1}, C_{Sp3}, discharged through the parallel capacitors.

Mode 2 [t_1<t<t_2]

As stated in the second mode in Fig. 3, S_2, S_4, and S_5 are turned on-state and body diodes of switches S_2, S_5, S_6 are on-state. The coupler capacitors C_2 and C_3 are charged and C_1 is discharged thorough input filter L_{f1} as seen in Fig. 2.b. The current flows through resonant tank series inductors L_{P1}, L_{P3}, and returns from

the series inductor L_{P2}. While, the parallel capacitors C_{Pp1} is charged, C_{Pp2} and C_{Pp3} are discharged. The current flows through the series capacitors and charges C_{Sp1} and C_{Sp3}, and C_{Sp2} is discharged through the series inductor L_{P2}. The current goes through the three-phase coupler transformer phase - A winding L_A, and returns from phase - B winding L_B and phase - C winding L_C to the series capacitor C_{Sp2}.

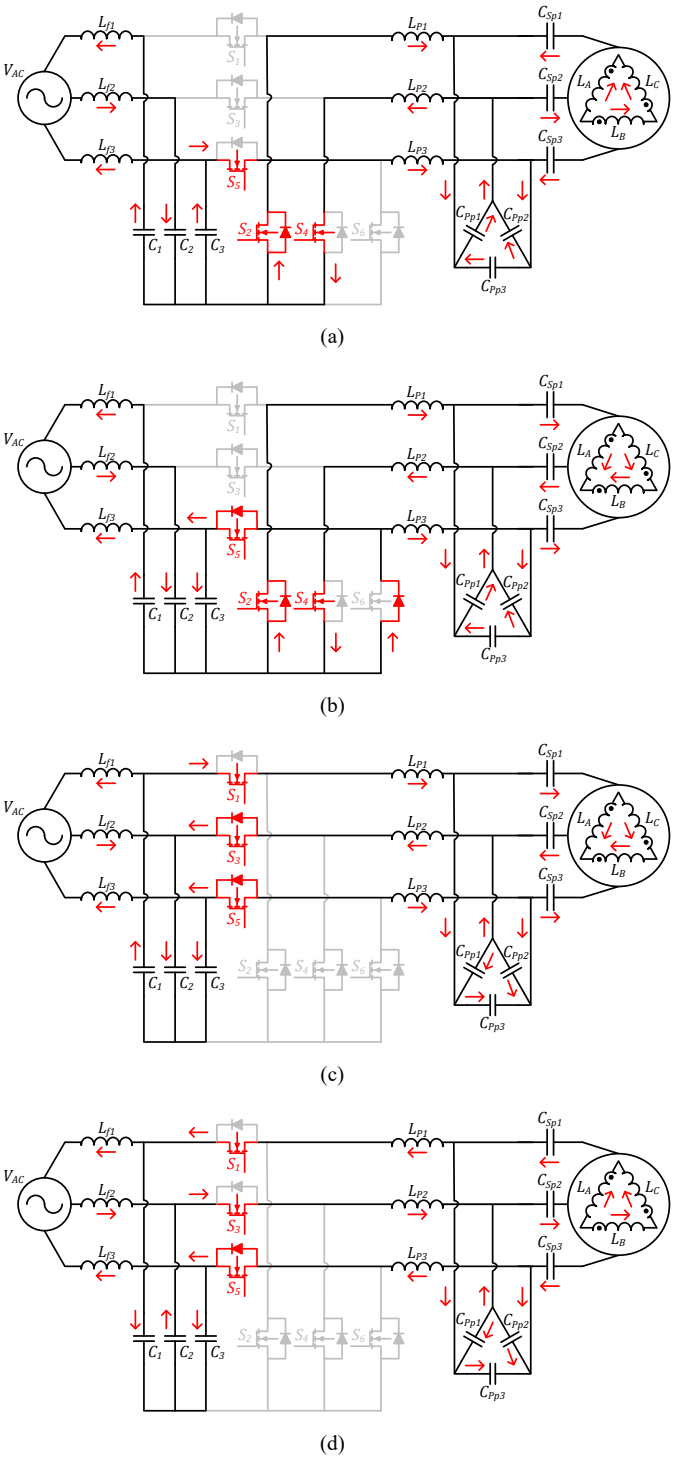

Fig. 2. Mode analysis, current path, and switching transition.

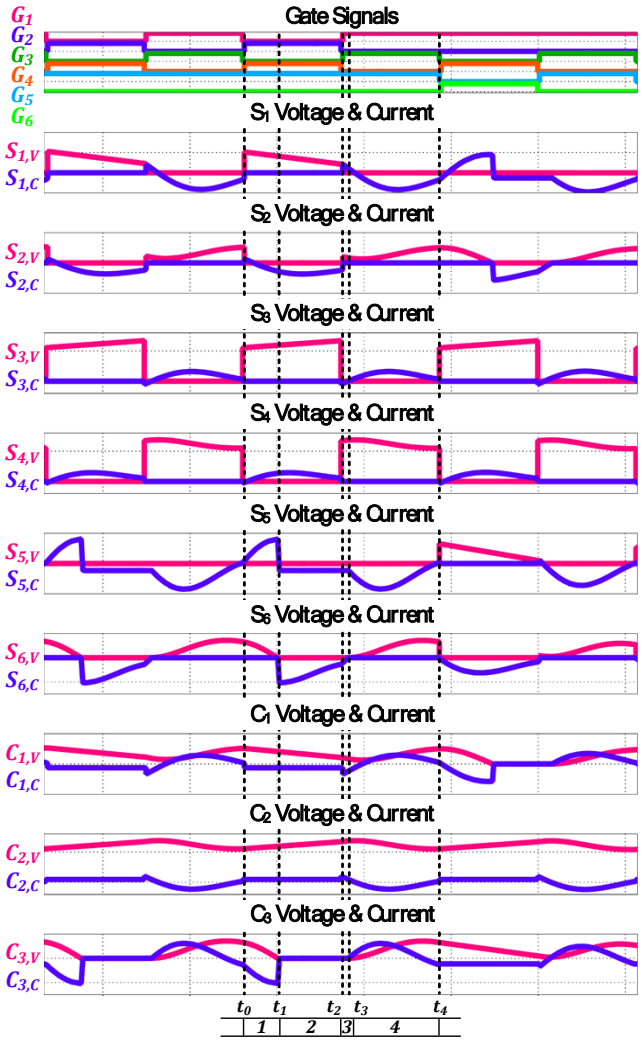

Fig. 3. Three phase voltage and current waveforms of the switches, and decoupling capacitors.

Mode 3 [t_2<t<t_3]

The converter active switches S_1, S_3, and S_5 are on-state, and body diodes of S_3 and S_5 are conducting in this interval as shown in Fig. 3. Similar to the previous mode, the coupler capacitors C_2 and C_3 are charged and C_1 is discharged. The resonant tank current flows through the series inductors L_{P1} and L_{P3} to the parallel capacitors and returns to series inductor L_{P2}. While the parallel capacitors C_{Pp2} and C_{Pp3} are charged and the parallel capacitor C_{Pp1} is discharged to the series inductor L_{P2}. The series capacitors C_{Sp1} and C_{Sp3} are charged and the first phase series capacitor C_{Sp2} is discharged to the series inductor L_{P2} as demonstrated in Fig. 2.c. The coupler coil current flows through the phase - A winding L_A and returns from phase - B winding L_B and phase - C winding L_C to the series capacitor C_{Sp2}.

Mode 4 [t3<t<t4]

As described in Fig. 3, the converter active switches S_1, S_3, and S_5 are on-state and body diode of S_5 are on-state in this

interval. The coupling capacitors C_1 and C_3 are charged and C_2 is discharged to the second phase series inductor L_{P2}. The resonant tank current returns from the first and third phase series inductors L_{P1}, L_{P3} to the coupling capacitors and input filter inductors as presented in Fig. 2.d. The parallel capacitor C_{Pp2} and C_{Pp3} are charged and the parallel capacitors C_{Pp1} is discharged through the second phase series capacitor C_{Sp2}. In this interval, the series capacitor C_{Sp2} is charged through the three-phase coupler transformer and the series capacitors C_{Sp1} and C_{Sp3} are discharged to the parallel capacitors and the series inductors L_{P1} and L_{P3}. The coupler coil current flows from phase - B winding L_B and phase - C winding L_C and returns from phase - A to the series capacitors C_{Sp1} and C_{Sp3}.

III. The Oak Ridge Converter System Analysis

The input phase voltages respect to the ground v_{an}, v_{bn}, v_{cn} of the proposed WPT system can be represented considering the three-phase balanced system with the rms values of the input phase voltages in time domain as,

$$v_{an}(t) = \sqrt{2}V_{an,rms}sin(2\pi f_{60}t), \quad (1)$$

$$v_{bn}(t) = \sqrt{2}V_{bn,rms}sin\left(2\pi f_{60}t + \frac{2\pi}{3}\right), \quad (2)$$

$$v_{cn}(t) = \sqrt{2}V_{cn,rms}sin\left(2\pi f_{60}t - \frac{2\pi}{3}\right). \quad (3)$$

where f_{60} is the fundamental of the grid frequency. The input phase currents of the system i_a, i_b, i_c can be described in time domain with the rms values of the input currents since the proposed converter can achieve the unity power factor,

$$i_a(t) = \sqrt{2}I_{a,rms}sin(2\pi f_{60}t), \quad (4)$$

$$i_b(t) = \sqrt{2}I_{b,rms}sin\left(2\pi f_{60}t + \frac{2\pi}{3}\right), \quad (5)$$

$$i_c(t) = \sqrt{2}I_{c,rms}sin\left(2\pi f_{60}t - \frac{2\pi}{3}\right). \quad (6)$$

The system decoupling capacitors should be designed at the maximum output power to provide the unity power factor at the minimum load conditions. The system phase powers p_a, p_b, p_c can be defined considering the decoupling capacitors charge and discharge of the energy within one switching period as,

$$p_a(t) = \frac{1}{2}C_1\left(\sqrt{2}V_{an,rms}sin(2\pi f_{60}t)\right)^2 f_{sw}, \quad (7)$$

$$p_b(t) = \frac{1}{2}C_2\left(\sqrt{2}V_{bn,rms}sin\left(2\pi f_{60}t + \frac{2\pi}{3}\right)\right)^2 f_{sw}, \quad (8)$$

$$p_c(t) = \frac{1}{2}C_3\left(\sqrt{2}V_{cn,rms}sin\left(2\pi f_{60}t - \frac{2\pi}{3}\right)\right)^2 f_{sw}, \quad (9)$$

where f_{sw} is the resonant system switching frequency. The total input instantaneous power can be calculated considering the equivalent amplitude of the phase voltages V_{ph} ($=V_{an,rms}=V_{bn,rms}=V_{cn,rms}$) and the same value of the decoupling capacitors C_d ($=C_1=C_2=C_3$) as,

$$p_{in}(t) = p_a(t) + p_b(t) + p_c(t) = C_d V_{ph}^2 \left[sin^2(2\pi f_{60}t) + sin^2\left(2\pi f_{60}t + \frac{2\pi}{3}\right) + sin^2\left(2\pi f_{60}t - \frac{2\pi}{3}\right)\right] f_{sw} \quad (10)$$

The total input average power can be obtained considering the unity power factor through the resonant compensation and wireless coupling coils to the output, and three-phase balanced system as,

$$P_{in} = \frac{3}{2}C_d V_{ph}^2 f_{sw} \quad (11)$$

The decoupling capacitor C_d value can be calculated averaging total output power P_O since the three phase input phase voltages V_{ph} are constant at the constant output power P_O as,

$$C_d = \frac{2P_O}{3V_{ph}^2 f_{sw}\eta} \quad (12)$$

where η is the efficiency of the proposed converter. The input filter inductor value L_f ($=L_{f1}=L_{f2}=L_{f3}$) of the system can be calculated considering the input impedance of the system seen from the output of the input filter. In order to avoid phase shift of input current, the filter inductor should be much lower than the input impedance of the proposed converter at the line frequency f_{60}. Since the input has unity power factor at the minimum load condition, the input impedance can be considered to be an almost resistive load, R_{in}. The minimum input impedance can be found at the maximum output power conditions and the filter inductor L_f is,

$$L_f \ll \frac{V_{ph}^2\eta}{2\pi f_{60}P_O} \quad (13)$$

The single-phase equivalent of the resonant tank circuit is demonstrated in Fig. 4.

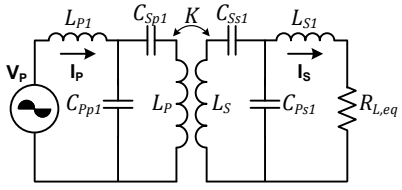

Fig. 4. Single-phase equivalent circuit of the resonant stage.

The phase input voltage v_P can be written as

$$v_P(t) = \frac{2}{\pi}V_{an,rms}sin(2\pi f_{60}t)\sum_{n=1,3,..}^{\infty}\frac{1}{n}sin(n2\pi f_{sw}t) \quad (14)$$

Since the system is balanced, the average magnitude of the equivalent input voltage V_P and the resonant tank phase current I_P ($=I_{P1}=I_{P2}=I_{P3}$) can be expressed as,

$$V_P = \frac{2}{\pi\sqrt{2}}V_{ph}, \quad I_P = \frac{\pi\sqrt{2}}{2}\frac{P_O}{\eta V_{ph}} \quad (15)$$

The equivalent primary and secondary inductances L_P, L_S of coupling transformer can be stated in matrix form as,

$$L_P = \begin{bmatrix} L_A & M_{AB} & M_{CA} \\ M_{AB} & L_B & M_{BC} \\ M_{CA} & M_{BC} & L_C \end{bmatrix},\ L_S = \begin{bmatrix} L_D & M_{DE} & M_{FD} \\ M_{DE} & L_E & M_{EF} \\ M_{FD} & M_{EF} & L_F \end{bmatrix} \quad (16)$$

where L_A, L_B, L_C are transmitter phase inductances and M_{AB}, M_{BC}, M_{CA} are mutual inductances between phases L_A and L_B, L_B and L_C, and L_C and L_A, respectively. While, L_D, L_E, L_F are receiver coil phase inductances, the M_{DE}, M_{EF}, and M_{FD} are the mutual inductances between phases L_D and L_E, L_E and L_F, and L_F and L_D, respectively. The coupler coil magnetizing inductance and leakage inductances of the transmitter coil L_{Lp} and receiver coil L_{Ls} can be computed with the coupling coefficient factor of K as,

$$L_M = K\sqrt{L_P L_S},\ L_{Lp} = L_P - L_M \text{ and } L_{Ls} = L_S - L_M \quad (17)$$

The equivalent load resistance $R_{L,eq}$ at the receiver side output can be obtained as,

$$R_{L,eq} = \frac{2V_{battery}^2}{3\ P_O} \quad (18)$$

The transmitter and receiver resonant network equation in a matrix form can be shown as

$$\begin{bmatrix} V_P \\ V_{battery} \end{bmatrix} = \begin{bmatrix} j\omega L_{P1} + \left[\frac{1}{j\omega C_{Pp1}} // \left(\frac{1}{j\omega C_{Sp1}} + j\omega L_{L,p} + j\omega L_M\right)\right] & -j\omega L_M \\ -j\omega L_M & j\omega L_M + \frac{1}{n^2}\left[j\omega L_{L,s} + \frac{1}{j\omega C_{Ss1}} + \left(\frac{1}{j\omega C_{Ps1}} // j\omega L_{S1}\right)\right] \end{bmatrix} \begin{bmatrix} I_P \\ I_S \end{bmatrix} \quad (19)$$

where $\omega = \{2\pi f_{sw}\}$ represents switching frequency of f_{sw} and n is the turns ratio between transmitter and receiver coils which is expressed by $n = \sqrt{L_S/L_P}$. The resonant frequency of the compensation system can be stated with the system components as,

$$\omega_o = 1/\sqrt{L_{P1}C_{Pp1}} = 1/\sqrt{L_{S1}C_{Ps1}} = 1/\sqrt{(L_P - L_{P1})C_{Sp1}} = 1/\sqrt{(L_S - L_{S1})C_{Ss1}} \quad (20)$$

The corresponding voltage transfer functions of the bi-directional system in charging mode can be expressed by

$$|M_{V,gain}| = \left|\frac{V_S}{V_P}\right| = \left|\frac{\omega^2 L_M C_{Pp1}}{\left(1 - (\omega/\omega_o)^2 + j\omega C_{Ss1}R_{L,eq}\right)\left(1/C_{PS1} + j\omega L_S\right) + j\omega L_{S1} + R_{in}}\right| \quad (21)$$

IV. Simulation Results

The design parameters of the proposed system for the simulation are summarized in Table I.

TABLE I - Simulated System Parameters

Symbol	Parameter	Value
V_{LAC}	ac input voltage	277 $V_{AC,RMS}$
V_O	dc output voltage	675 V_{DC}
P_O	output power	35 kW
L_i	input filter inductor	1.2 mH
C_d	decoupling capacitor	2.33 µF
L_{Ps}	primary series inductor	4.27 µH
C_{Pp}	primary parallel capacitor	255 nF
C_{Ps}	primary series capacitor	340 nF
L_P	primary self-inductances	42 µH
L_S	secondary self-inductances	42 µH
C_{Ss}	secondary series capacitance	340 nF
C_{Sp}	secondary parallel capacitance	255 nF
L_{Ss}	secondary series inductor	4.27 µH
k	coupling co-efficient	0.15
C_e	decoupling capacitor	0.34 µF
L_C	common mode choke	200 µH
f_{60}	grid frequency	60 Hz
f_{SW}	operating frequency	88.5 kHz
t_{dead}	dead time	600 ns

The proposed Oak Ridge converter system simulation results are provided from three-phase grid system to the battery at 35 kW, 277 $V_{AC,RMS}$ input, and 675 V_{DC} output voltages as presented in Fig. 5. The resonant tank and input / output filter components are computed from theoretical calculation as discussed above. Furthermore, the three-phase coupling coils are simulated for a coupling factor of 0.15 considering 6 inches air gap based on the experimental measurement. The input three-phase current THD is obtained around 5% with 0.99 PF as seen from the simulation result in Fig. 5 (a). As demonstrated in Fig. 5 (b), the three-phase grid frequency is transferred to the dc voltage and current in the receiver side by the proposed unique converter. Fig. 3 (c) shows the first phase resonant tank voltage and current waveforms across primary and secondary resonant tank input / output terminals. The grid frequency is superimposed with the high switching frequency component through the proposed converter, resonant stage, and coupling coils and transferred to the receiver as shown in the figure. The primary and secondary resonant voltage and current waveforms are zoomed and presented in Fig. 3 (d). The resonant tank transmitter is at the resonant frequency with third harmonic injected as seen in the zoomed in current waveform at the primary side. The transferred power through the coupling coils is rectified through the diodes and filtered with the rectifier output capacitor and the filter common mode choke inductor before connection to the battery terminals. High frequency zoomed in voltage and current waveforms across the secondary resonant tank can be seen as in Fig. 3 (d).

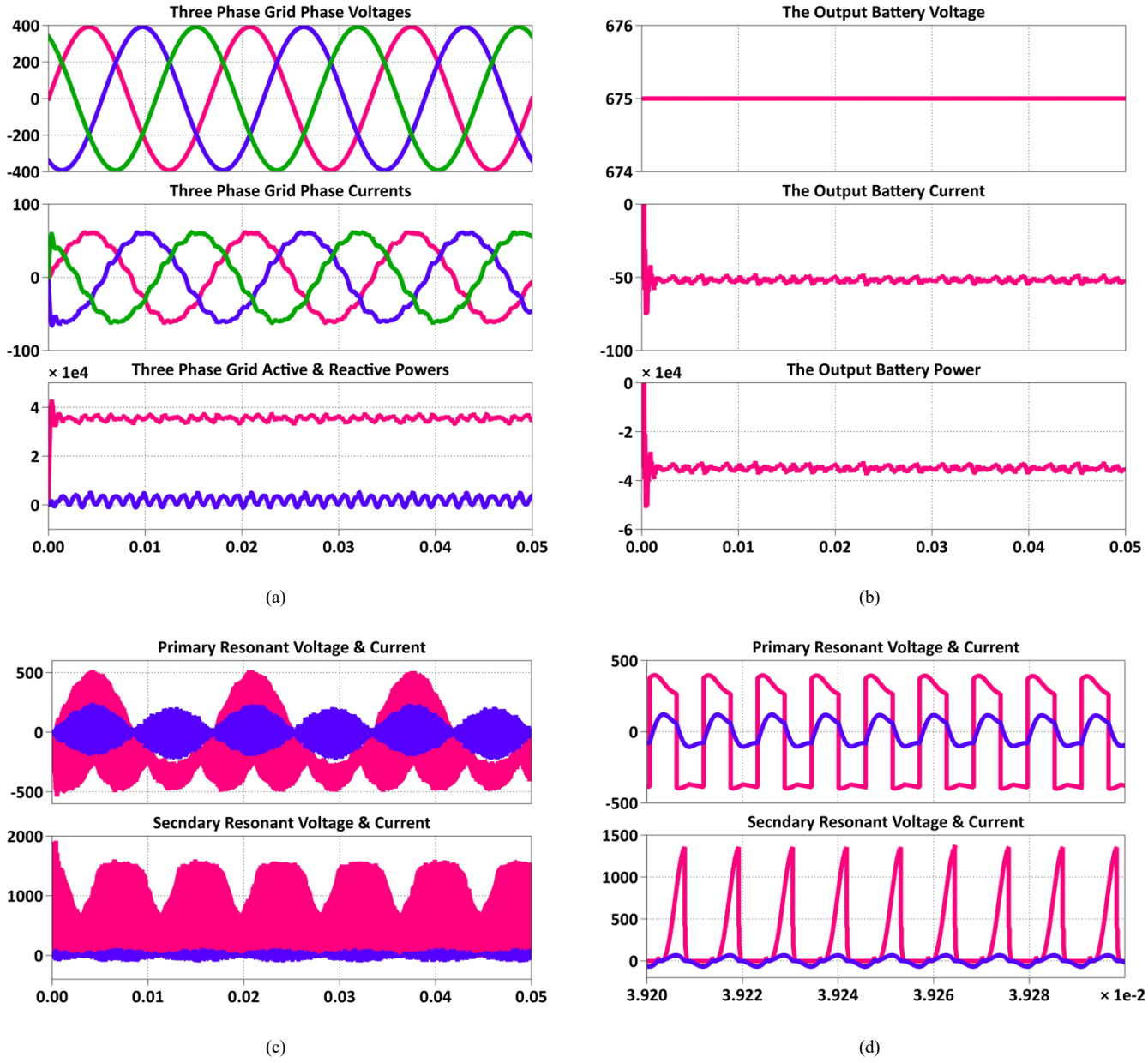

Fig. 5. Simulation results of the proposed system with grid to energy storage power flow: (a) grid side three-phase voltages, currents, and active & reactive power, b) energy storage side three-phase voltages, currents, and active & reactive power, c) primary and secondary side resonant tank voltage & current waveforms, d) zoomed-in view of primary and secondary side resonant tank voltage and current waveforms.

V. CONCLUSIONS

A new patent pending ac/dc Oak Ridge converter is presented for wireless charging of electric vehicles in this paper. One of the major advantages of the proposed system is that it does not require a front-end PFC rectifier which is required in conventional charging systems. The proposed converter topology is presented in this paper with the state analysis and switching transitions through the active and passive components. The proposed system theoretical analysis is described by design equations from the input filter to the resonant components and three-phase coupling coils. The system simulation analysis is also demonstrated at the target power showing the input grid and output voltage / current waveforms with the grid active / reactive and output powers. The primary / secondary resonant tank voltage and current waveforms are simulated showing the hybrid grid and high frequency components. The three-phase grid power with an input voltage of 277 $V_{AC,RMS}$ is transferred to the receiver output across the battery terminals at a battery voltage of 675 V_{DC}. The target output power is obtained at the output of 35 kW achieving 5% THD and 0.98 power factor on the grid side. The 60 Hz

frequency three-phase grid input is inverted to the high-frequency signal by Oak Ridge converter and power transfer is achieved through the coupler coil system and resonant compensation to the output for battery charging as demonstrated. The proposed converter technology can eliminate the front-end PFC rectification stage ensuring high power quality on the grid side with harmonics and high-power factor with less number of active and passive components with reduced number of power conversion stage designs.

ACKNOWLEDGEMENTS

This project is funded by Oak Ridge National Laboratory's Laboratory Directed Research and Development (LDRD) Program's Transformational Energy Science and Technology (TEST) initiative with the project ID LOIS-9505. This research used resources available at the Power Electronics and Electric Machinery Research Center located at the National Transportation Research Center, a DOE EERE User Facility operated by the Oak Ridge National Laboratory (ORNL). The authors would like to thank the TEST Initiative Lead, Dr. Ilias Belharouak for his support of this work and his guidance. Authors also acknowledge the support and guidance of ORNL Sustainable Transportation Program Manager, Dr. Rich Davies, which is greatly appreciated.

REFERENCES

[1] J. Pries, V. P. N. Galigekere, O. C. Onar, and G. Su, "A 50-kW three-phase wireless power transfer system using bipolar windings and series resonant networks for rotating magnetic fields," *IEEE Transactions on Power Electronics*, vol. 35, no. 5, pp. 4500-4517, May 2020.

[2] D. Patil, M. K. McDonough, J. M. Miller, B. Fahimi, and P. T. Balsara, "Wireless power transfer for vehicular applications: Overview and challenges," *IEEE Transactions on Transportation Electrification*, vol. 4, no. 1, pp. 3-37, Mar. 2018.

[3] A. Khaligh and M. D'Antonio, "Global trends in high-power on-board chargers for electric vehicles," *IEEE Transactions on Vehicular Technology*, vol. 68, no. 4, pp. 3306-3324, Apr. 2019.

[4] A. Greifelt, B. Rubey, and D. Gerling, "High temperature superconductor based 500 kW smart grid charging for mobile applications," in *Proc., IEEE Vehicle Power and Propulsion Conference (VPPC)*, pp. 1-5, December 2017, Belfort, France.

[5] V. Cirimele, M. Diana, F. Bellotti, R. Berta, N. E. Sayed, A. Kobeissi, P. Guglielmi, R. Ruffo, M. Khalilian, A. L. Ganga, J. Colussi, and A. D. Gloria, "The FABRIC ICT platform for managing wireless dynamic charging road lanes," *IEEE Transactions on Vehicular Technology*, vol. 69, no. 3, pp. 2501-2512, Mar. 2020.

[6] M. Bojarski, E. Asa, K. Colak, and D. Czarkowski, "Analysis and control of multiphase inductively coupled resonant converter for wireless electric vehicle charger applications," *IEEE Transactions on Transportation Electrification*, vol. 3, no. 2, pp. 312-320, Jun. 2017.

[7] J. M. Miller, O. C. Onar, and M. Chinthavali, "Primary-side power flow control of wireless power transfer for electric vehicle charging," *IEEE Journal of Emerging and Selected Topics in Power Electronics*, vol. 3, no. 1, pp. 147-162, Mar. 2015.

[8] M. Moghaddami, A. Anzalchi, and A. I. Sarwat, "Single-stage three-phase AC–AC matrix converter for inductive power transfer systems," *IEEE Transactions on Industrial Electronics*, vol. 63, no. 10, pp. 6613-6622, Oct. 2016.

[9] J. Noeren, N. Parspour, and B. Sekulic, "A direct matrix converter with space vector modulation for contactless energy transfer systems," in *Proc., IEEE 18th International Power Electronics and Motion Control Conference (PEMC)*, pp. 22-27, August 2018, Budapest, Hungary.

[10] N. Xuan Bac, D. M. Vilathgamuwa, and U. K. Madawala, "A SiC-based matrix converter topology for inductive power transfer system," *IEEE Transactions on Power Electronics*, vol. 29, no. 8, pp. 4029-4038, Aug. 2014.

[11] H. L. Li, A. P. Hu, G. A. Covic, "A direct AC–AC converter for inductive power-transfer systems," *IEEE Transactions on Power Electronics*, vol. 27, no. 2, pp. 661-668, Feb. 2012.

[12] J. Liu, K. W. Chan, C. Y. Chung, N. H. L. Chan, M. Liu, and W. Xu, "Single-stage wireless-power-transfer resonant converter with boost bridgeless power-factor-correction rectifier," *IEEE Transactions on Industrial Electronics*, vol. 65, no. 3, pp. 2145-2155, Mar. 2018..

[13] S. Samanta and A. K. Rathore, "A new inductive power transfer topology using direct AC–AC converter with active source current waveshaping," *IEEE Transactions on Power Electronics*, vol. 33, no. 7, pp. 5565-5577, Jul. 2018.

[14] M. Moghaddami and A. I. Sarwat, "Single-phase soft-switched AC–AC matrix converter with power controller for bidirectional inductive power transfer systems," *IEEE Transactions on Industry Applications*, vol. 54, no. 4, pp. 3760-3770, July-Aug. 2018.

[15] S. Weerasinghe, U. K. Madawala, and D. J. Thrimawithana, "A matrix converter-based bidirectional contactless grid interface," *IEEE Transactions on Power Electronics*, vol. 32, no. 3, pp. 1755-1766, Mar. 2017.

[16] N. S. González-Santini, H. Zeng, Y. Yu, and F. Z. Peng, "Z-source resonant converter with power factor correction for wireless power transfer applications," *IEEE Transactions on Power Electronics*, vol. 31, no. 11, pp. 7691-7700, Nov. 2016.

[17] J. Liu, W. Xu, K. W. Chan, M. Liu, X. Zhang, and N. H. L. Chan, "A three-phase single-stage AC–DC wireless-power-transfer converter with power factor correction and bus voltage control," *IEEE Journal of Emerging and Selected Topics in Power Electronics*, vol. 8, no. 2, pp. 1782-1800, Jun. 2020.